Modeling and analysis of I-V hysteresis behaviors caused by defects in tin perovskite thin films

Taishi Noma, Dai Taguchi, Takaaki Manaka, and Mitsumasa Iwamoto[a)]
Department of Electrical and Electronic Engineering, Tokyo Institute of Technology, 2-12-1 O-okayama, Meguro-ku, Tokyo 152-8552, Japan

(Received 1 August 2018; accepted 20 October 2018; published online 7 November 2018)

We analyzed the I-V hysteresis behaviors of tin perovskite ($MASnI_3$, MA: CH_3NH_3) thin films using impedance spectroscopy coupled with charge modulation spectroscopy (CMS). The capacitance-voltage (C-V) characteristics of the ITO/$MASnI_3$/Al device showed hysteresis behaviors, in accordance with the trap filling process suggested by the I-V characteristics. The CMS measurement indicated the enlargement of the energy bandgap of the $MASnI_3$. On the basis of these results, we proposed a model that trap states in the vicinity of the bottom of conduction band are filled, and concluded that the trap filling process occurring at Sn vacancies makes a significant contribution to the electrical properties of tin perovskite film and the hysteresis of the I-V and C-V characteristics of our device. The I-V hysteresis is suppressed with the decrease of defects such as Sn vacancies in $MASnI_3$ films. *Published by AIP Publishing.* https://doi.org/10.1063/1.5050557

I. INTRODUCTION

Recently, organolead halide perovskite ($CH_3NH_3PbI_3$, $MAPbI_3$) solar cells have attracted much attention in energy harvesting engineering, because high power conversion efficiency (PCE) solar cells are fabricated at low cost.[1] Nevertheless, the use of toxic lead (Pb) is strictly restricted in the world, particularly by the European Union. It is necessary to fabricate lead-free solar cells. As lead-free perovskite solar cell materials, tin perovskite such as $CH_3NH_3SnI_3$ ($MASnI_3$) is one of the most promising candidates.[2,3] However, tin perovskite films suffer from chemical instability, pin-holes, non-uniformity, and so on. Accordingly, many studies have been devoted to the improvement of the preparation process of solar cells[4,5] and the synthesis of new tin perovskite materials such as $FASnI_3$,[6] $CsSnI_3$,[7] 2D tin perovskite,[8] and others. Nevertheless, the PCE of these tin perovskite solar cells is still quite low (9%[8]), and it is actually very low in comparison with lead perovskite solar cells (22.7%[9]).

The PCE is dependent on the photovoltaic mechanism of solar cells. For lead perovskite solar cells, many ideas have been proposed to elucidate the highly efficient photovoltaic mechanism as follows: exciton binding energy at room temperature is very low (ca. 5 meV[10,11]), and it is comparable to that of crystal-Si. The ferroelectricity of $MAPbI_3$ at room temperature efficiently contributes to form carrier pathways.[12,13] In $MAPbI_3$ films, intrinsic defects do not form the states which can act as trap centers within the bandgap, and this leads to long-range diffusion of carriers.[14] Ion migration directly gives effects on the I-V hysteresis of the solar cells,[15] and the photovoltaic effect is deteriorated accordingly. On the basis of these ideas, the fundamental physical and electrical properties of tin perovskite solar cells have also been investigated, on paying attention to the photovoltaic efficiency. The electron mobility of $MASnI_3$ is $\mu = 2320\ cm^2/Vs$[16] and the diffusion length L is longer than 500 nm,[17] and these values are much greater than those of $MAPbI_3$.[16,18] Nevertheless, the actual impact of using $MASnI_3$ on the photovoltaic effect has not been experimentally demonstrated in association with defects, ion migration, ferroelectricity, etc. In the case of solid-state ionic crystals including perovskite, lattice defects serve as electron trapping sites and ion transport pathways. Actually, owing to the high defect density of $MASnI_3$,[19] I^- and MA^+ can move with low activation energies, in the manner same as in $MAPbI_3$.[20,21] We therefore believe that it is important to clarify the photovoltaic mechanism of tin perovskite solar cells, with taking into account carrier traps and ion migration.

In this study, we analyzed the I-V hysteresis behaviors observed for lead-free tin perovskite $MASnI_3$ thin films, by using impedance spectroscopy coupled with charge modulation spectroscopy (CMS). Impedance spectroscopy gives the information on the dielectric polarization, and CMS measurement elucidates the energetics of $MASnI_3$.[22] We then modeled the I-V hysteresis behaviors taking into account the trap filling process and ion migration.

II. EXPERIMENTAL METHODS

Figure 1(a) shows the structure of ITO/$MASnI_3$/Al, prepared using a spin-coating method. SnI_2 (1.0M), CH_3NH_3I (Methylammonium iodide, MAI) (1.0M), and SnF_2 (0.3M) were mixed in γ-butyrolactone (GBL)/dimethyl sulfoxide (DMSO) mixed solvent (7:3 v/v). The resulting solution was used for the spin-coating of lead-free perovskite, after filtering using a 0.45 μm polytetrafluoroethylene (PTFE) filter. This solution was spin-coated on patterned ITO-coated glass substrates in an N_2-filled glove box, with a rotation speed of 1500 rpm for 60 s. After this spin-coating, anti-solvent toluene was dropped onto the film to promote the perovskite crystal formation. Subsequently, the spin-coated film was again rotated at 3000 rpm for 60 s to completely evaporate

[a)]E-mail: iwamoto@pe.titech.ac.jp

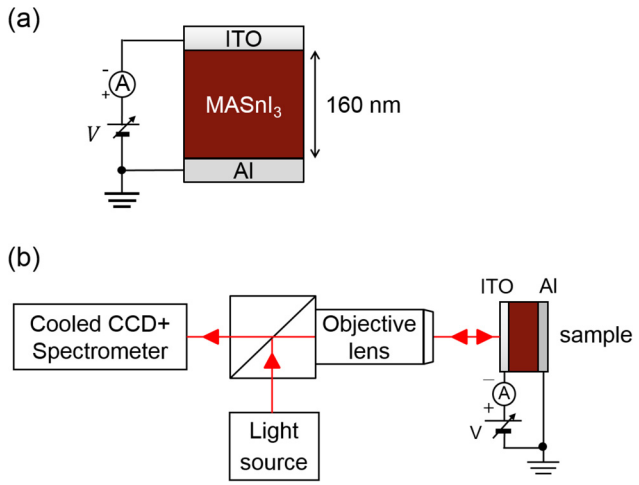

FIG. 1. (a) The sample structure and (b) experimental setup of the CMS measurement.

residual toluene, followed by thermal annealing at 100 °C for 10 min. The resulting spin-coated films on the ITO were $MASnI_3$ film, onto which Al electrode was thermally evaporated with a thickness of 100 nm. The prepared ITO/$MASnI_3$/Al devices were encapsulated using a cover glass, where the working area of the device was approximately 3.1 mm^2.

The I-V measurement was conducted using a source meter (Keithley 2400), with a scan speed of 0.08 V/s. We applied the DC voltage to the ITO electrode with reference to the Al electrode of the ITO/$MASnI_3$/Al device. The capacitance-frequency (C-f) and capacitance-voltage (C-V) characteristics were measured using an impedance analyzer (Solartron SI 1260), by applying small AC signals of 100 mV.

In the CMS measurement, a white light from a halogen lamp was passed through an objective microscope lens and focused onto the device perpendicularly from the ITO electrode side [see Fig. 1(b)], where the spot area was 100 μm in diameter and light intensity was 89 mW/cm^2. The reflected light was collected with a spectrometer (Andor Technology: SR-163) attached to a cooled charge-coupled device image sensor (Andor Technology: DU-920P-BV) in the region between 340 nm and 850 nm in wavelength.

III. RESULTS AND DISCUSSION

A. C-f characteristics and Nyquist plots

Figure 2(a) shows the C-f characteristics of the sample in the frequency region from 1 MHz to 100 mHz under zero DC bias. The measurement was conducted in dark at room temperature. At the frequency region around 100 kHz, a plateau appears, and at lower frequency region, the capacitance C significantly increases by more than 1 order with the decrease of frequency f. The film thickness of our device is estimated to be about 160 nm, by using the relative dielectric constant of $MASnI_3$ ($\varepsilon_{eff} = 23$).[23] The significant increase of the capacitance observed in the low frequency region is due to the long-range ion migration,[24] but ionic electrode polarization due to the condensation of ions around the electrode also contributes to that increase.[25] Figure 2(b) shows the Nyquist plots of our device. Results suggest that the diffusion-like transport expressed as Warburg impedance [$Z = (R/C)^{1/2}(j\omega)^{-1/2}$] governs our device.[26] That is, diffusion-like Warburg behavior is dominant and carriers do not spread homogeneously over the bulk region at the frequencies of 100 mHz < f < 1 MHz under zero bias. With consideration of these, we may argue that the carrier transfer in the $MASnI_3$ film can be modeled using a transmission line model [see Fig. 2(c)], and this model accounts well for the significant frequency dependence of the capacitance seen in Fig. 2(a). This diffusion-like carrier transport supports the long-range movement of ions and electrons/holes in the $MASnI_3$ film, where I^- and MA^+ ions are possible candidates.[20,21]

B. CMS spectra

Figure 3 shows the CMS spectra at various DC voltages, where the relative change in the reflection spectrum [$-\Delta R/R = (I_0 - I)/I_0$] was simultaneously recorded during the I-V measurement. That is, DC voltage was cyclically scanned in a manner as 0 V → +4 V → 0 V → −4 V → 0 V. The intensity I_0 was determined at 0 V, prior to this scanning. The $-\Delta R/R$ represents the absorption of the bulk of $MASnI_3$ film by assuming that the incident light passes through the ITO and $MASnI_3$ successively and finally reaches the Al electrode.

When increasing the DC voltage from 0 V to +4 V, the $-\Delta R/R$ decreased below 0 at the wavelength region longer than 550 nm. The decrease of the $-\Delta R/R$ can be attributed to filling of trap states by the applied DC voltage, and the electron excitation to this energy states by the light is prohibited after the trap states are filled. We will discuss the trap filling in Subsection III C. From the viewpoint of the DC voltage dependence of the absorption spectra, we can assume that the residual SnI_2 in the $MASnI_3$ film has many trap states, where the energy bandgap of SnI_2 is 2.275 eV (i.e., 544 nm in optical wavelength)[27] and the $-\Delta R/R$ changes broadly around the wavelength region corresponding to this bandgap energy (i.e., in the region longer than 550 nm).

In the negative DC voltage region such as at −3 V and −4 V, the $-\Delta R/R$ took positive values and did not return to 0 after the forward scan of the DC voltage (−4 V → 0 V). This is possibly due to the release of carriers originally trapped in the as-deposited film or due to the increase of trap states themselves during the application of negative voltage. Interestingly, the CMS spectra at around 800 nm in Fig. 3 showed that the $-\Delta R/R$ returns to 0 without taking positive values. Here, the wavelength of 800 nm corresponds to the absorption edge and the bandgap ($E_g = 1.55$ eV) of the $MASnI_3$ (see Fig. 6 in the Appendix), under the assumption that $MASnI_3$ is a direct bandgap semiconductor.[28] This result suggests that in the as-deposited film, carriers are not trapped at the states close to the conduction band E_c of the $MASnI_3$, possibly due to the establishment of thermodynamic equilibrium between the trap states and the conduction band. Therefore, the $-\Delta R/R$ at 800 nm indicates reversible trap filling, and this may reflect the electrical properties of the $MASnI_3$ film. With taking into account these, the hysteresis behavior of the $-\Delta R/R$ at 800 nm will be further discussed in Subsection III C.

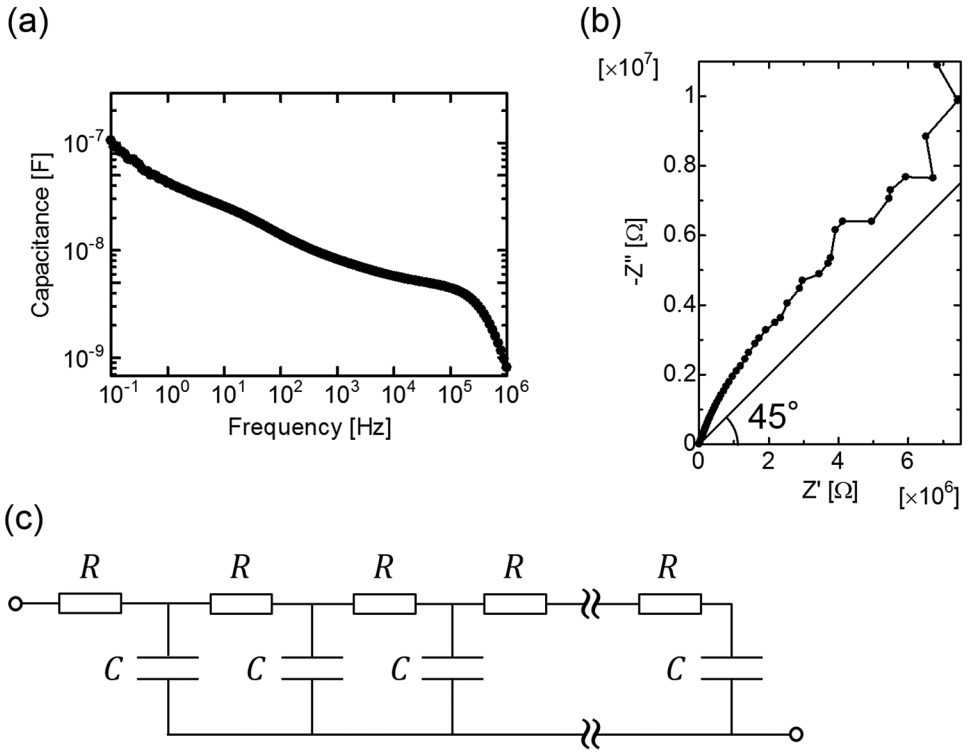

FIG. 2. (a) C-f characteristics, (b) Nyquist plots of the device, and (c) a transmission line model.

For the explanation of the increase of trap states, we here provide a possibility that traps were increased by the oxidation of Sn^{2+} during the voltage application. Sn^{2+} in $MASnI_3$ and in residual SnI_2 is easily oxidized to Sn^{4+}, accompanying the formation of Sn vacancies that can act as trap sites.[29] Accordingly, the increase of $-\Delta R/R$ caused by the oxidation of Sn^{2+} will happen during voltage application. In that case, the $-\Delta R/R$ does not return to 0 after the completion of one scan cycle, because Sn^{4+} is chemically more stable than Sn^{2+}.

C. Hysteresis behaviors of $MASnI_3$

The I-V, C-V, and CMS measurements were conducted to analyze the hysteresis behaviors of $MASnI_3$ films. Figure 4(a) shows the I-V characteristics, which we measured together with the CMS measurement. The I-V curve showed a rectifying behavior with hysteresis loops. The current level is low at voltages in the direction of the scan from 0 V to +4 V, in comparing with the current level at voltages in the direction of the scan from +4 V to 0 V (hysteresis loop is anti-clockwise direction). On the other hand, the current level is high at voltages in the direction of the scan from 0 V to −4 V, in comparing with the current level at voltages in the direction of the scan from −4 V to 0 V (hysteresis loop is anti-clockwise direction). Many researchers have pointed out that this kind of rectifying behavior with S-shape hysteresis loop is the result of resistive switching of perovskite, and this switching is available for resistive random access memory (ReRAM).[30–32] As to the resistive switching mechanisms of lead perovskite, many models have been proposed. Among them are models based on trapping/detrapping process,[30] ion migration across the vacancies,[31] and metal filaments.[32] In other words, there are many models that account for the switching, possibly owing to the differences of perovskite materials ($MAPbI_3$, $MAPbI_{3-x}Cl_x$, $MAPbBr_3$, etc.), device configurations, and preparation processes.

For our $MASnI_3$ device, the ratio between high resistance state and low resistance state is less than 10 (in the

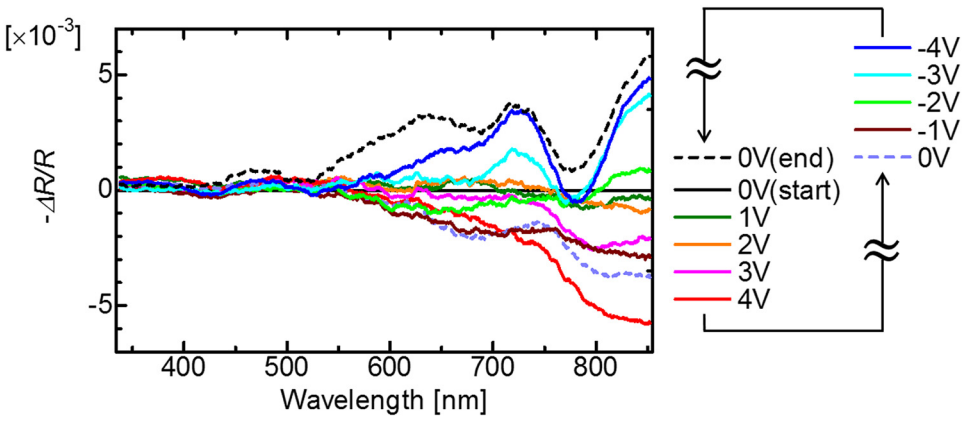

FIG. 3. The CMS spectra at various applied DC voltages.

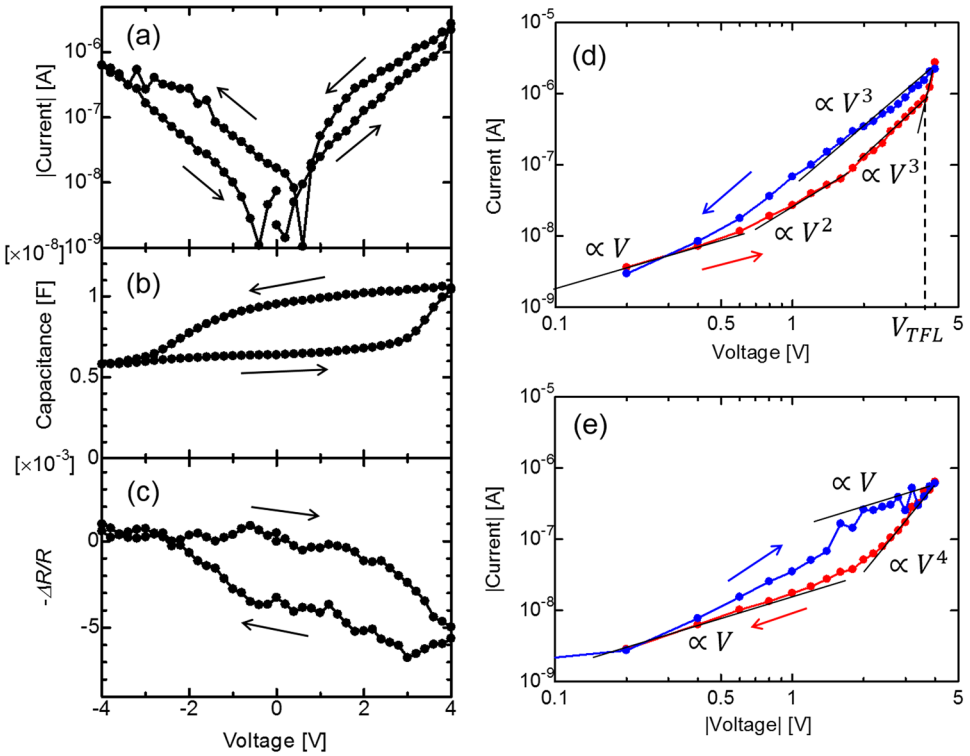

FIG. 4. [(a)–(c)] The hysteresis behaviors of the $MASnI_3$ thin film. (a) I-V, (b) C-V characteristics, and (c) the voltage dependence of the CMS modulation at 800 nm. [(d) and (e)] The log-log plots of the I-V characteristics in (d) positive and (e) negative voltage region.

positive and negative bias regions), and this ratio is too small in the light of the on/off ratio of the so-called resistive switching. Therefore, filamentary paths formed by ion migration and metal electrodes do not seem to be a main contributor for the rectifying behavior with S-shape hysteresis loop. Furthermore, the results of C-V and CMS measurements also suggest that filamentary paths are not the case of the hysteresis of our device, which will be discussed in the following part. We believe that the trap filling process significantly contributes to the I-V hysteresis. As discussed in the CMS spectra, trap filling process occurs at defects such as Sn vacancies in a film and leads to the increase of the current flowing across the film, in a way suggested by the space-charge limited current (SCLC) theory on insulators.[33]

Here, we pay attention to the reversible S-shaped hysteresis behavior, but there are several possibilities that account for the behavior. One possibility is the non-radiative recombination between electrons and holes, where holes (or electrons) trapped at defects during the positive voltage application vanish due to the recombination with electrons (or holes) which are injected from the electrode during the negative voltage application. Ion migration which involves trap filling may also be one of the possibilities, since ions can reversibly move across the film along the direction of applied DC field and heal trap centers on defects. Assuming that defects locally distribute near the electrodes, the trap centers on the defects are filled with ions which are migrated from the counter electrode. In that case, electron/hole injection will be enhanced, and the direction of the I-V hysteresis loop should be anti-clockwise in the positive voltage region and should be clockwise in the negative voltage region. However, our result in Fig. 4(a) does not support this idea, where the direction of the loop in the negative region is anti-clockwise. Furthermore, there is no direct evidence of the distribution of defects in space and the identification of ion species. We believe that the trap filling process accompanying non-radiative recombination is the most possible process that explains our results.

With consideration of these, we propose a model that accounts for the S-shape hysteresis on the basis of the theory of carrier transport of insulating films,[33] by using log-log plots as shown in Figs. 4(d) and 4(e). Figures 4(d) and 4(e) show the log I-log V plots of the I-V characteristics, where the contribution of the displacement current $C\mathrm{d}V/\mathrm{d}t$ was removed from the experimental I-V data.

Figure 4(d) plots the positive voltage region, where the I-V hysteresis is seen. In the low voltage region ($V < +1$ V), ohmic current I flows in proportion to V. In the middle voltage region ($+1\ \mathrm{V} \le V \le +2\ \mathrm{V}$), the current I increases in proportion to V^2. This behavior corresponds to the space-charge limited current (SCLC) that flows across insulators. For insulating films with single carrier traps, it can be written as

$$I = \frac{9}{8}\varepsilon\varepsilon_0\mu\theta S\frac{V^2}{d^3}, \tag{1}$$

with $\theta = n/N_t$, under the assumption that the quasi-thermodynamic equilibrium is established between free carrier density n and trap density N_t in insulators. Here, ε, ε_0, μ, S, and d represent relative dielectric constant, vacuum permittivity, carrier mobility, electrode area, and film thickness, respectively. For our $MASnI_3$ device, we obtain $\mu\theta = 1.6 \times 10^{-9}\ \mathrm{cm}^2/\mathrm{Vs}$ from Fig. 4(d). The effective carrier mobility $\mu\theta$ is very low.

In the case when traps are energetically distributed, current I increases in a manner as $I \propto V^n$ $(n \ge 3)$ due to the filling of shallow traps followed by deep traps.[33] Noteworthy, our experiment shows that the current I increases in a manner as $I \propto V^3$ in the region between +2 V

and +3.6 V [see Fig. 4(d)]. After all the traps are filled ($V > V_{TFL} = +3.6$ V), the current I abruptly increases because injected carriers can freely move in the film without being trapped. Here, V_{TFL} is the trap-filled limit voltage needed to fill all trap states, which can be expressed as[33]

$$V_{TFL} = \frac{eN_t d^2}{2\varepsilon\varepsilon_0}, \tag{2}$$

where e and N_t represent elementary charge and the density of all trap states, respectively. $N_t = 3.7 \times 10^{17}$ cm^{-3} was obtained from Eq. (2), under the assumption that the relative dielectric constant of $MASnI_3$ is $\varepsilon = 23$. The obtained trap density is one order higher than that of solution-processed lead perovskite films.[34] When the applied voltage is scanned in the direction from +4 V to 0 V, the current I decreases in a manner as $I \propto V^3$, following the trap-filled SCLC model.[33] At this stage, the current level is still high because the traps remain filled. This is a most possible reason for the S-shaped hysteresis in the positive bias region. Note that our devices were electrically broken at around +5 V, and the maximum voltage we could apply to the device was +4 V in the measurement.

Figure 4(e) shows the negative voltage region. When the voltage decreases from 0 V, the trap-filled SCLC I flows ($I \propto V^n$ $n > 1$). In the region of $-2\text{ V} > V > -4$ V, this current is suppressed ($I \propto V$). That is, the filled traps vanish due to non-radiative recombination with the injected carriers with opposite polarity, resulting in empty trap states. In the region from −4 V to 0 V, the current I sharply decreases and the current level drops owing to the presence of empty traps that can capture carriers, subsequently ohmic current I ($I \propto V$) flows. In this way, we can explain the S-Shaped hysteresis in the negative bias region.

Figure 4(b) shows the C-V characteristics obtained by scanning DC bias voltage in a manner as 0 V → +4 V → 0 V → −4 V → 0 V under AC signals of 100 mV with 1 kHz. At the starting point of the measurement (0 V), the capacitance was approximately 6 nF, whose value well agrees with the value obtained from the C-f characteristic [Fig. 2(a)]. That is, this value corresponds to the capacitance where diffusion-like transport is dominant, denoted as C_0. Interestingly, it was found that the capacitance C starts to increase in the region >+3 V when we scan from 0 V to +4 V, while C is nearly constant in the region of $0\text{ V} < V < +3$ V. At around the V_{TFL} (=+3.6 V) where all traps are filled [see Fig. 4(d)], the capacitance most significantly increases. In this region (>+3 V), injected electronic carriers significantly contribute to increase the capacitance. The specific feature of the C-V hysteresis of our device is that the capacitance C does not exceed $2C_0$. This feature can be explained by using a trap filling model, in the way same as in references.[33] This feature is easy to understand if injected carriers uniformly spread over the film and the film behaves like a conductor, the centroid of injected carriers positions in the center of the film, in film thickness direction. Noteworthy, carriers which are injected and reaching the counter electrode do not contribute to the increase of capacitance but contribute to the increase of conductance. Furthermore, the increased capacitance does not change while the DC bias decreases from +4 V to 0 V, and the capacitance C returns to the original value C_0 while the voltage decreases in the region 0 V → −4 V [see Fig. 4(b)]. These results of the C-V characteristics suggest that the capacitance increases due to a trap filling process and not due to filamentary paths which are partially and non-uniformly formed in the electrode area.

Figure 4(c) shows the voltage dependence of CMS at 800 nm, which was obtained from the CMS spectra in Fig. 3. Interestingly, the hysteresis behavior of the $-\Delta R/R$ at 800 nm was reversible and similar to the hysteresis behaviors of the I-V and C-V curves. In the CMS measurement, only a partial and small region (7.9×10^{-5} cm^2) of the whole electrode area (3.1×10^{-2} cm^2) was measured. Therefore, the similarity to the I-V and C-V hysteresis suggests that filamentary paths might not be a physical reason for the hysteresis of our device.

In the hysteresis loop, we can see the decrease of the absorption ($-\Delta R/R < 0$). If the absorption around the absorption edge decreases, the absorption spectrum should be blue shifted and the energy bandgap between the conduction band minimum and the valence band maximum should be enlarged. Therefore, this decrease of the $-\Delta R/R$ at 800 nm is regarded as the enlargement of the energy bandgap of the $MASnI_3$. We argue that this enlargement of energy bandgap is due to the filling of trap states, located close to the conduction band of the $MASnI_3$.[35] Taking into account the experimental results of I-V, C-V, and CMS, it is reasonable that the increase of the current I and capacitance C and the decrease of the absorption are interpreted as the contribution of the trap filling. Note that dielectric polarization does not influence CMS spectra; therefore, we successfully distinguished the trap filling from the dielectric polarization of $MASnI_3$. On the other hand, the enlargement of the bandgap of perovskite has been already reported as the Burstein-Moss effect,[36,37] which is normally observed in semiconductors. Handa *et al.* reported that the addition of SnF_2 to $MASnI_3$ results in hole doping and causes the blue shift of the absorption edge. Based on these reports, the bottom of the conduction band is elevated by the increased carrier concentration n due to the trap filling, resulting in the blue shift of the absorption edge. However, our modulation is only on the order of 10^{-3} which is much smaller than that reported in Ref. 37. Additionally, the bandgap shift ΔE_g should be significantly changed with the increase of the current I, because the relationship $\Delta E_g \propto n^{2/3}$ is satisfied between the bandgap shift and carrier concentration. With consideration of these, we believe that the main physical reason for the CMS hysteresis is trap filling, but not Burstein-Moss effect.

From these results, we propose the following model that accounts for the hysteresis behavior of our device (see Fig. 5). This model is composed of two regions: (i) trap-unfilled region (0 V → +3.6 V, −2 V → −4 V → 0 V) and (ii) trap-filled region (+3.6 V → +4 V → −2 V). In Fig. 5, we regarded the trap sites as Sn vacancies, because Sn vacancies are the most probable trap sites in $MASnI_3$. In $MASnI_3$, the formation energy of Sn vacancies is very low and Sn vacancies are inevitable dominant defects.[19] As we pointed out in C-f characteristics shown in Fig. 2(a), Sn vacancies are

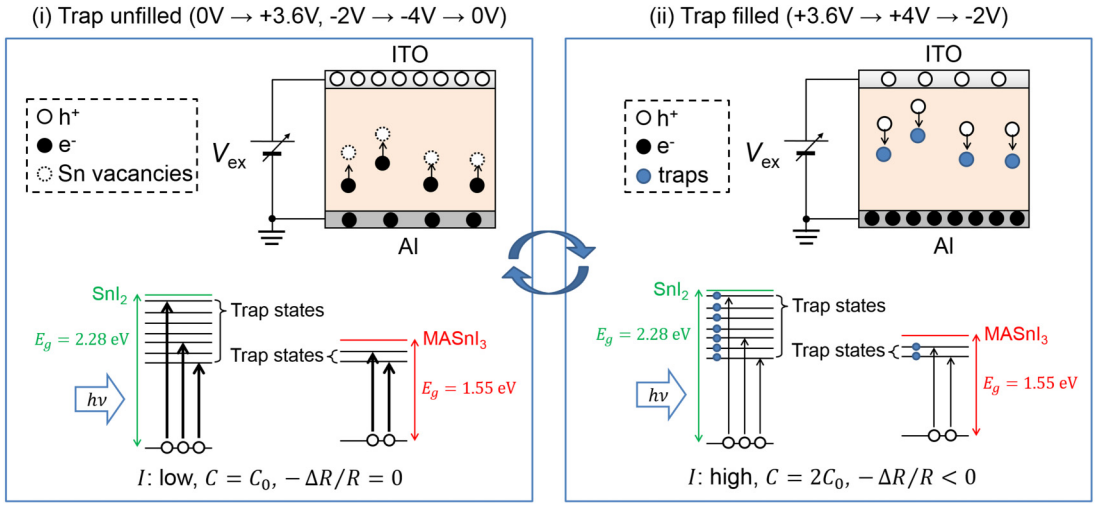

FIG. 5. The schematic image of the model of hysteresis behaviors. (i) trap unfilled region (0 V → +3.6 V, −2 V → −4 V → 0 V) and (ii) trap filled region (+3.6 V → +4 V → −2 V). It is assumed that the Sn vacancies serve as a non-radiative recombination center. For simplicity, the excitation to the conduction band and the influence of oxidation of Sn^{2+} are ignored in the figure.

immobile, whereas I^- and MA^+ are mobile. For simplicity, the influence of oxidation of Sn^{2+} is ignored in Fig. 5. (i) When the voltage V is increasing from 0 V, trap states are still unfilled and shallow traps are gradually filled by injected carriers. Therefore, the current level is low, $C = C_0$ and $-\Delta R/R$ gradually decreases from 0. Subsequently, when deep traps are filled at around +3 V, the current increases in a manner as $I \propto V^n$ $(n \geq 3)$ and the $-\Delta R/R$ sharply decreases. The capacitance gradually increases due to the excessive injected carriers. (ii) After the trap states are fully filled at around +3.6 V, the current I abruptly increases and the current level changes to a high level, and the decrease of $-\Delta R/R$ becomes moderate. At the same time, the capacitance C continuously increases to $2C_0$ until the injected carriers homogeneously distribute in the film. When the voltage V is decreasing from +4 V to 0 V, the traps remain filled because they cannot be released by the positive voltage; therefore, the current level, capacitance C, and absorption $-\Delta R/R$ do not change. When the voltage V further decreases from 0 V to −4 V, the capacitance gradually decreases because the traps become unfilled due to the recombination with the injected carriers with opposite polarity. At the same time, the $-\Delta R/R$ increases to 0 as the bandgap narrows. (i) After all the trap states become empty at around −2 V, the current level goes down and the capacitance decreases to C_0. Note that we can see that the $-\Delta R/R$ has already returned to 0 at around −2 V. When the voltage V is scanned from −4 V to 0 V, the current level, capacitance C, and $-\Delta R/R$ do not change since the trap states remain unfilled.

IV. CONCLUSION

We investigated the I-V hysteresis behaviors of $MASnI_3$ in C-V measurement coupled with CMS measurement. I-V hysteresis was modeled on the basis of the trap filling process in insulating films. Our model comprehensively accounts for the hysteresis behaviors in terms of electrical properties and carrier energetics. From the C-V measurement, we argued that polarization is apparently enhanced by the carrier injection caused by trap filling. This trap filling process also accounts for the reversible hysteresis behavior under the assumption of the non-radiative recombination at defects. The CMS measurement more strongly supported the model for the I-V and C-V hysteresis, in terms of the trap filling process involving the energy bandgap enlargement. It has been clarified that the trap filling which occurs at Sn vacancies makes a significant contribution to the hysteresis. Our results showed that defects such as Sn vacancies in $MASnI_3$ should be decreased to suppress the I-V hysteresis. We believe that the investigation of electronic traps and ion migration will promote the development of lead-free perovskite solar cells.

ACKNOWLEDGMENTS

This work was supported by JSPS KAKENHI (Grant Nos. 17J00264 and 18H01473).

APPENDIX: DETERMINATION OF ABSORPTION EDGE

We obtained the absorption edge of the $MASnI_3$ film from the absorption spectrum, using the relationship satisfied

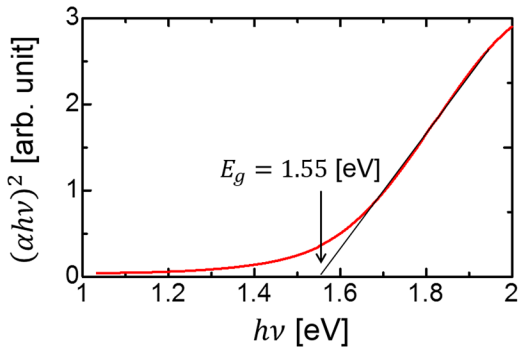

FIG. 6. The absorption edge of the $MASnI_3$ obtained from the absorption spectrum.

for direct bandgap semiconductors.

$$\alpha \propto (h\nu - E_g)^{1/2}/h\nu, \quad (h\nu > E_g), \tag{A1}$$

where E_g is the energy bandgap. Figure 6 clearly shows that the absorption edge of the $MASnI_3$ is 800 nm ($E_g = 1.55$ eV), corresponding to the wavelength at which we plotted the voltage dependence of the CMS in Fig. 4(c).

[1]T. Miyasaka, Chem. Lett. **44**, 720 (2015).
[2]F. Hao, C. C. Stoumpos, D. H. Cao, R. P. H. Chang, and M. G. Kanatzidis, Nat. Photonics **8**, 489 (2014).
[3]N. K. Noel, S. D. Stranks, A. Abate, C. Wehrenfennig, S. Guarnera, A.-A. Haghighirad, A. Sadhanala, G. E. Eperon, S. K. Pathak, M. B. Johnston, A. Petrozza, L. M. Herz, and H. J. Snaith, Energy Environ. Sci. **7**, 3061 (2014).
[4]T. Fujihara, S. Terakawa, T. Matsushima, C. Qin, M. Yahiro, and C. Adachi, J. Mater. Chem. C **5**, 1121 (2017).
[5]M. Xiao, S. Gu, P. Zhu, M. Tang, W. Zhu, R. Lin, C. Chen, W. Xu, T. Yu, and J. Zhu, Adv. Opt. Mater. **6**, 1700615 (2018).
[6]W. Liao, D. Zhao, Y. Yu, C. R. Grice, C. Wang, A. J. Cimaroli, P. Schulz, W. Meng, K. Zhu, R.-G. Xiong, and Y. Yan, Adv. Mater. **28**, 9333 (2016).
[7]M. H. Kumar, S. Dharani, W. L. Leong, P. P. Boix, R. R. Prabhakar, T. Baikie, C. Shi, H. Ding, R. Ramesh, M. Asta, M. Graetzel, S. G. Mhaisalkar, and N. Mathews, Adv. Mater. **26**, 7122 (2014).
[8]S. Shao, J. Liu, G. Portale, H.-H. Fang, G. R. Blake, G. H. ten Brink, L. J. A. Koster, and M. A. Loi, Adv. Energy Mater. **8**, 1702019 (2018).
[9]M. A. Green, Y. Hishikawa, E. D. Dunlop, D. H. Levi, J. Hohl-Ebinger, and A. W. Y. Ho-Baillie, Prog. Photovolt. Res. Appl. **26**, 427 (2018).
[10]J. Even, L. Pedesseau, and C. Katan, J. Phys. Chem. C **118**, 11566 (2014).
[11]A. Miyata, A. Mitioglu, P. Plochocka, O. Portugall, J. T. Wang, S. D. Stranks, H. J. Snaith, and R. J. Nicholas, Nat. Phys. **11**, 582 (2015).
[12]J. M. Frost, K. T. Butler, F. Brivio, C. H. Hendon, M. van Schilfgaarde, and A. Walsh, Nano Lett. **14**, 2584 (2014).
[13]H.-S. Kim, S. K. Kim, B. J. Kim, K.-S. Shin, M. K. Gupta, H. S. Jung, S.-W. Kim, and N.-G. Park, J. Phys. Chem. Lett. **6**, 1729 (2015).
[14]J. Kim, S. H. Lee, J. H. Lee, and K. H. Hong, J. Phys. Chem. Lett. **5**, 1312 (2014).
[15]Z. Xiao, Y. Yuan, Y. Shao, Q. Wang, Q. Dong, C. Bi, P. Sharma, A. Gruverman, and J. Huang, Nat. Mater. **14**, 193 (2015).
[16]C. C. Stoumpos, C. D. Malliakas, and M. G. Kanatzidis, Inorg. Chem. **52**, 9019 (2013).
[17]L. Ma, F. Hao, C. C. Stoumpos, B. T. Phelan, M. R. Wasielewski, and M. G. Kanatzidis, J. Am. Chem. Soc. **138**, 14750 (2016).
[18]S. D. Stranks, G. E. Eperon, G. Grancini, C. Menelaou, M. J. P. Alcocer, T. Leijtens, L. M. Herz, A. Petrozza, and H. J. Snaith, Science **342**, 341 (2013).
[19]T. Shi, H. Zhang, W. Meng, Q. Teng, M. Liu, X. Yang, Y. Yan, H.-L. Yip, and Y. Zhao, J. Mater. Chem. A **5**, 15124 (2017).
[20]C. Eames, J. M. Frost, P. R. F. Barnes, B. C. O'Regan, A. Walsh, and M. S. Islam, Nat. Commun. **6**, 7497 (2015).
[21]S. Meloni, T. Moehl, W. Tress, M. Franckevičius, M. Saliba, Y. H. Lee, P. Gao, M. K. Nazeeruddin, S. M. Zakeeruddin, U. Rothlisberger, and M. Graetzel, Nat. Commun. **7**, 10334 (2016).
[22]T. Otsuka, D. Taguchi, T. Manaka, and M. Iwamoto, J. Appl. Phys. **121**, 065501 (2017).
[23]P. Umari, E. Mosconi, and F. De Angelis, J. Phys. Chem. Lett. **9**, 620 (2018).
[24]M. Iwamoto, J. Appl. Phys. **77**, 5314 (1995).
[25]O. Almora, I. Zarazua, E. Mas-Marza, I. Mora-Sero, J. Bisquert, and G. Garcia-Belmonte, J. Phys. Chem. Lett. **6**, 1645 (2015).
[26]M. Bag, L. A. Renna, R. Y. Adhikari, S. Karak, F. Liu, P. M. Lahti, T. P. Russell, M. T. Tuominen, and D. Venkataraman, J. Am. Chem. Soc. **137**, 13130 (2015).
[27]H. Yoshida, N. Ohno, and M. Fujita, Phys. Status Solidi **203**, 281 (1997).
[28]P. Umari, E. Mosconi, and F. De Angelis, Sci. Rep. **4**, 4467 (2014).
[29]S. Gupta, D. Cahen, and G. Hodes, J. Phys. Chem. C **122**, 13926 (2018).
[30]E. J. Yoo, M. Lyu, J.-H. Yun, C. J. Kang, Y. J. Choi, and L. Wang, Adv. Mater. **27**, 6170 (2015).
[31]D. J. Kim, Y. J. Tak, W.-G. Kim, J. K. Kim, J. H. Kim, and H. J. Kim, Adv. Mater. Interfaces **4**, 1601035 (2017).
[32]K. Yan, M. Peng, X. Yu, X. Cai, S. Chen, H. Hu, B. Chen, X. Gao, B. Dong, and D. Zou, J. Mater. Chem. C **4**, 1375 (2016).
[33]M. A. Lampert and P. Mark, *Current Injection in Solids* (Academic Press, New York, 1970).
[34]N. K. Noel, A. Abate, S. D. Stranks, E. S. Parrott, V. M. Burlakov, A. Goriely, and H. J. Snaith, ACS Nano **8**, 9815 (2014).
[35]Y. Shao, Z. Xiao, C. Bi, Y. Yuan, and J. Huang, Nat. Commun. **5**, 5784 (2014).
[36]J. S. Manser and P. V. Kamat, Nat. Photonics **8**, 737 (2014).
[37]T. Handa, T. Yamada, H. Kubota, S. Ise, Y. Miyamoto, and Y. Kanemitsu, J. Phys. Chem. C **121**, 16158 (2017).